Journal of Power Sources 263 (2014) 332–337

Contents lists available at ScienceDirect

Journal of Power Sources

journal homepage: www.elsevier.com/locate/jpowsour

Short communication

Investigation of $(1-x)LiMnPO_4 \cdot xLi_3V_2(PO_4)_3/C$: Phase composition and electrochemical performance

Chenyun Wang, Yujing Bi, Yang Liu, Yinping Qin, Yanqun Fang, Deyu Wang*

Ningbo Institute of Materials Technology and Engineering, Chinese Academy of Science, 519 Zhuangshi Road, Ningbo, Zhejiang 315201, China

HIGHLIGHTS

- Thoroughly investigation on the phase composition of $(1-x)LiMnPO_4 \cdot xLi_3V_2(PO_4)_3/C$.
- Plough-shape tendency of composites' capacities as the increase of $Li_3V_2(PO_4)_3$ phase.
- "Gaining point" identified as 20% $Li_3V_2(PO_4)_3$ incorporation.

ARTICLE INFO

Article history:
Received 30 December 2013
Received in revised form
24 March 2014
Accepted 11 April 2014
Available online 24 April 2014

Keywords:
Phosphate composite
Mutual-substituted bi-phase mixture
$LiMnPO_4$
$Li_3V_2(PO_4)_3$
Lithium-ion batteries

ABSTRACT

Here we report the characteristics of mutual-substituted bi-phase composites with nominal formula of $(1-x)LiMnPO_4 \cdot xLi_3V_2(PO_4)_3/C$ ($x = 0.01, 0.03, 0.05, 0.1, 0.15, 0.2, 0.3, 0.4, 0.5$). According to the results of refinement and XPS, as $x \geq 0.03$, the prepared material becomes the binary mixture of $LiMn_{1-y}V_yPO_4$ and $Li_3V_{2-z}Mn_z(PO_4)_3$ where y is probably ramped rapidly and z is relatively stable. Tested between 2.5–4.4 V *vs.* Li/Li^+, the electrochemical performance of the synthetic composites presents the Plough-shape tendency as the increase of $Li_3V_2(PO_4)_3$'s nominal ratio. The discharge capacity is dropped from 99 mAh g^{-1} of $0.99LiMnPO_4 \cdot 0.01Li_3V_2(PO_4)_3/C$ to 69 mAh g^{-1} for $0.95LiMnPO_4 \cdot 0.05Li_3V_2(PO_4)_3/C$, then recuperated, and finally stabilized at ~125 mAh g^{-1} for the samples with 20% $Li_3V_2(PO_4)_3$ or more. Compared with $LiMnPO_4/C$, the "gaining point" of composites is incorporating 20% $Li_3V_2(PO_4)_3$, probably corresponding to ~8% vanadium substitution based on refinement results.

1. Introduction

The interest in lithium-ion batteries is driven by the increased market demand for portable electronics, transportation and energy storage. A strong research effort has been focused on developing new cathode materials to improve its safety, cyclic life, as well as cost-effectiveness [1]. Recently, there was a new trend to ameliorate the cathode's performance via complexing another property-complementary material to compromise the advantages and disadvantages of each other. For example, the mixture of $LiNi_{0.8}Co_{0.15}Al_{0.05}O_2$ and $LiMn_2O_4$ presented much better all-round properties in term of capacity, safety, Mn dissolution, and so on [2]. Indeed the combination of $LiNi_{0.5}Co_{0.2}Mn_{0.3}O_2 + LiCoO_2$ was widely used in smart-phone batteries as a result of the conflicts of energy density, rate capability and cost.

Olivine phosphates were regarded as one of the most promising cathodes in large format batteries to power the vehicles and shape the grids due to its high reversible capacity (170 mAh g^{-1}), good chemical & thermal stability and super-stable cyclability. $LiMnPO_4$, the other most promising member of olivine phosphates, gained ever-increasing attentions from academic community and industry due to its redox potential of 4.1 V *vs.* Li/Li^+, 0.65 V higher than that of $LiFePO_4$, indicating a higher energy density in practical cells [3–6].

NASICON (for Na^+ super-ionic conductor) phosphate $Li_3V_2(PO_4)_3$ is another important phosphate cathode owing to the higher Li^+ ion mobility and reasonable capacities in contrast to $LiFePO_4$ and $LiMnPO_4$. Li^+ ions could be removed at the redox potentials of 3.65, 3.7, 4.1 and 4.55 V *vs.* Li/Li^+ corresponding to the extraction of the first half, the second half, the 2nd and 3rd Li^+ ions. Restricted by the stability of state-of-art electrolyte, the 3rd Li^+ ion is hardly utilized in practical devices, namely the reversible capacity is *ca.* 131 mAh g^{-1} in theory [7–16].

Complexion of high-rate $Li_3V_2(PO_4)_3$ and potential high-capacity $LiFePO_4$ has been utilized to form a novel cathode

* Corresponding author.
E-mail addresses: wangdy@nimte.ac.cn, wdy770316@hotmail.com (D. Wang).

http://dx.doi.org/10.1016/j.jpowsour.2014.04.044
0378-7753/

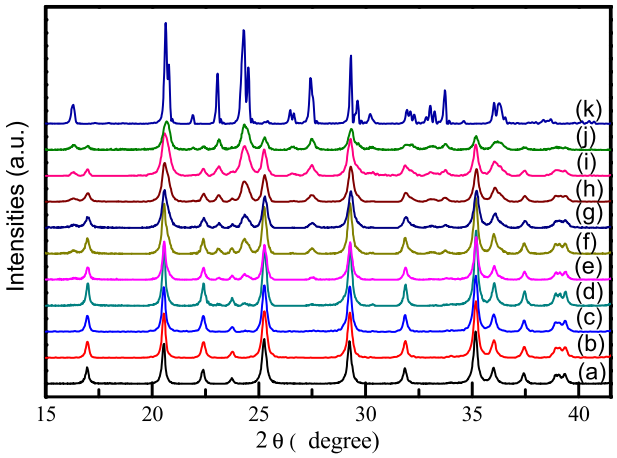

Fig. 1. XRD patterns of the synthetic samples. (a) LMP, (b) 0.99LMP·0.01LVP, (c) 0.97LMP·0.03LVP, (d) 0.95LMP·0.05LVP, (e) 0.9LMP·0.1LVP, (f) 0.85LMP·0.15LVP, (g) 0.8LMP·0.2LVP, (h) 0.7LMP·0.3LVP, (i) 0.6LMP·0.4LVP, (j) 0.5LMP·0.5LVP, (k) LVP.

composite with the acceptable multi-aspect characteristics [17–21]. The same strategy was also adopted to improve the performance of $LiMnPO_4$. In the proposed works [22–24], the discharge capacities of composites were almost monotonic augmented as the increase of NASICON phase. However, we noticed that the cells were charged to 4.5 V or higher potential, where 3rd Li^+ ion was involved into the reaction. As a result, the practical capacity of $Li_3V_2(PO_4)_3$ could target a value of 180–190 mAh g^{-1}. In other word, it was still ambiguous for the influence of $Li_3V_2(PO_4)_3$ on composites' performance in potentially practical application.

In addition, the composite should be the mixture of $LiMn_{1-y}V_yPO_4$ and $Li_3V_{2-z}Mn_z(PO_4)_3$ according to the previous works [22,23,25]. Although this structural characteristic was noticed, the phase composition and probable microstructure of the composites were not carefully investigated till date.

In this work, the composites of $(1-x)LiMnPO_4{\cdot}xLi_3V_2(PO_4)_3/C$ ($x = 0.01, 0.03, 0.05, 0.1, 0.15, 0.2, 0.3, 0.4$ and 0.5) are synthesized and thoroughly characterized in our laboratory. According to refinement and XPS, the composites are identified as the mixture of $LiMn_{1-y}V_yPO_4$ and $Li_3V_{2-z}Mn_z(PO_4)_3$, where y is increased rapidly from ~2% to ~20%, and z is slightly dropped from ~6% to ~4%. The prepared composites are electrochemically evaluated between 2.5–4.4 V *vs.* Li/Li^+ to exclude the influence of the 3rd Li^+ ion in NASICON phase. In contrast to the proposed works where discharge capacities were monotonically improved [22–24], the discharge performance presents the Plough-shape tendency as the increase of $Li_3V_2(PO_4)_3$'s nominal ratio. Also incorporating appropriate amount of $Li_3V_2(PO_4)_3$ can improve the rate capability and cyclist ability of the composites, instead of discharge capacity.

2. Experimental

The composites of $(1-x)LiMnPO_4{\cdot}xLi_3V_2(PO_4)_3/C$ (abbreviated as $(1-x)$LMP·xLVP, $x = 0.01, 0.03, 0.05, 0.1, 0.15, 0.2, 0.3, 0.4$ and 0.5) were prepared via high-temperature solid-state reaction. All chemicals were purchased from Aldrich with 99% purity. A mixture of LiH_2PO_4, $MnCO_3$ and NH_4VO_3 in a stoichiometric ratio was ground with 15 wt% sugar by high energy ball-milling for 4 h. Then the mixture was sintered in a tube furnace with the flowing gas of $Ar-H_2$ (92:8, v/v) at 350 °C for 10 h and cooled down to room temperature. After reground for another 4 h, the mixture was calcined at 600 °C for 20 h in the tube furnace with the flowing gas of $Ar-H_2$. The obtained material was ball-milled with 20 wt% Ketjenblack for 4 h to further improve the surface electronic conductivity and stored for electrochemical evaluation. $LiMnPO_4$ and $Li_3V_2(PO_4)_3$ were prepared in the same process as a control.

A slurry of *N*-methyl pyrrolidone (NMP) composing the prepared composite, poly(vinylidene fluoride) (PVDF) and super-P (8:1:1, w/w) was prepared and casted on an aluminum current collector. After drying at 120 °C under vacuum overnight, the electrodes were punched into 1.54 cm^2 disks with an average loading of 5 mg cm^{-2}. The CR2032 coin-cells were assembled with the prepared electrodes as cathode, Li foil as anode, Celgard 2550® as separator, and 1 M LiPF6 in ethylene carbonate (EC) + dimethyl carbonate (DMC) (1:1, v/v) as electrolyte. The assembly of the coin-cells was performed in an M-Braun glove box where humidity and oxygen were controlled less than 1 ppm.

The electrochemical evaluations were conducted on Land 2000 electrochemical measurement systems under room temperature. The cells for rate tests were cycled between 2.5 V and 4.4 V *vs.* Li/Li^+. It was set of 1 C current density as 170 mA g^{-1}, and the capacity was calculated based on the pure composite materials excluding carbon.

The crystallography phases were characterized by X-ray diffraction (XRD) with Cu Kα radiation (Bruker AXS, D8 Advance) with a scanning rate of 0.017° per second between 10–135°. The refinements were conducted with GSAS. It should be noted that the refined data was obtained after system could not be optimized any more. The morphologies of prepared samples were observed with scanning electron microscopy (SEM, Hitachi S-4800), and their microstructures were examined by transmission electron microscopy (TEM) on an FEI Tecnai F20 equipped with a field emission gun at an accelerating voltage of 200 kV. Surface analysis was conducted with a PHI 3056 X-ray Photoelectron Spectroscopy (XPS) which was excited by an Mg Kα radiation at a constant power of 100 W (15 kV and 6.67 mA). XPS spectrum was analyzed with GASA. The amount of carbon was determined on Vario EL (Elementar, Germany). Electrochemical impedance spectroscopy (EIS) was carried out in a frequency range from 0.01 Hz to 100 kHz with an Electrochemical Analyzer (Model 600D Series, CH Instruments).

Table 1
Phase ratio and substitute amount of olivine and NASICON in the synthetic composites.

Nominal ratio	Olivine		NASICON		wRp	Rp	CHI^2
	Ratio, %	TM ratio	Ratio, %	TM ratio			
0.99LMP·0.01LVP	100	$Mn_{0.980}V_{0.020}$	/	/	1.73	1.35	1.819
0. 7LMP·0.03LVP	99.21	$Mn_{0.970}V_{0.030}$	0.79	/	1.72	1.33	1.726
0.95LMP·0.05LVP	96.95	$Mn_{0.969}V_{0.031}$	3.05	$V_{1.886}Mn_{0.114}$	3.04	2.33	1.772
0.9LMP·0.1LVP	92.27	$Mn_{0.958}V_{0.042}$	7.73	$V_{1.884}Mn_{0.116}$	3.10	2.40	1.368
0.85LMP·0.15LVP	87.97	$Mn_{0.943}V_{0.057}$	12.03	$V_{1.894}Mn_{0.106}$	2.90	2.24	1.711
0.8LMP·0.2LVP	84.24	$Mn_{0.917}V_{0.083}$	15.76	$V_{1.879}Mn_{0.121}$	2.69	2.06	1.624
0.7LMP·0.3LVP	72.60	$Mn_{0.811}V_{0.189}$	27.40	$V_{1.927}Mn_{0.073}$	2.92	2.24	1.97
0.6LMP·0.4LVP	64.68	$Mn_{0.759}V_{0.241}$	35.32	$V_{1.916}Mn_{0.084}$	3.90	2.99	1.311
0.5LMP·0.5LVP	59.05	$Mn_{0.765}V_{0.235}$	40.95	$V_{1.926}Mn_{0.074}$	2.74	2.15	2.267

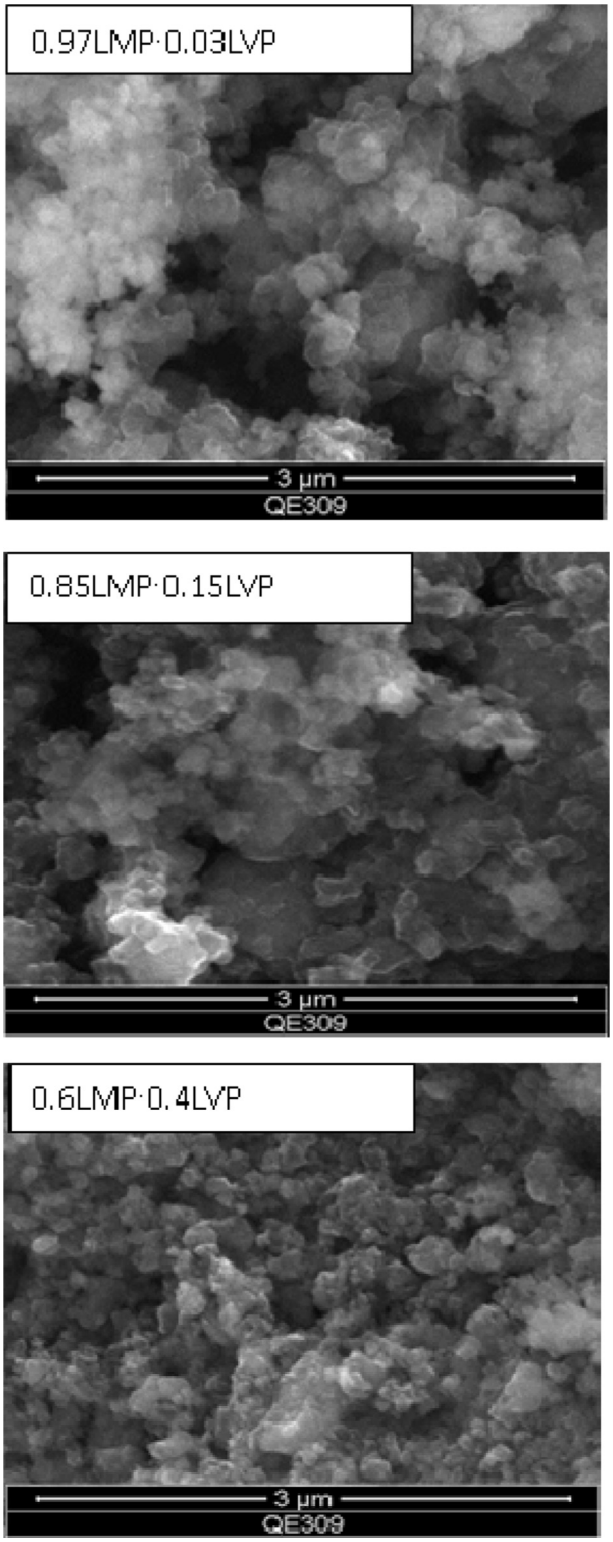

Fig. 2. SEM images of selected composite samples.

3. Results and discussion

Fig. 1 shows the XRD patterns of the prepared composites. The material with the nominal formula of 0.99LMP·0.01LVP/C is identified as pure olivine phase. NASICON phase starts to appear in the sample of 0.97LMP·0.03LVP/C, and gradually intensifies as the increase of vanadium amount. As the mutual substitution is probably taken place in the investigated composites, the mole ratio of both phases and the substitute amount were calculated via refinement with GSAS. As shown in Table 1 where the obtained results were compared, the replacing amount of vanadium in olivine structure is almost monotonic augmenting from 2% to ~20% as the increase of $Li_3V_2(PO_4)_3$'s nominal ratio, whereas manganese substitution is fluctuated around 5% in the whole range. In addition, the ratio of NASICON phase is a little lower than the nominal, indicating more vanadium atoms enter into the olivine lattice. Although the mutual-doping amount from refinement was semi-quantitative, it was a best way to reveal the variation of the composites' microstructure.

All composites present a similar irregular morphology with a size of 200–500 nm, as shown in Fig. 2. Carbon contents in the prepared samples are around 5.5 wt% tested via Vario EL. To understand the microstructure of the composites, 0.6LMP·0.4LV/C is selected to be characterized with HRTEM (Fig. 3). The observed particles are coated by a layer of amorphous carbon with a thickness of ~6 nm. The observed particles could be attributed to NASICON phase or olivine structure, namely one particle only has one phase instead of the mixture. For example, Particle a & b are identified as NASICON phase and olivine phase with selected area electron diffraction (SAED), as shown in Fig. 3a1 & b1 and the related crystallographic information listed in Table 2. As shown in Fig. 3a2, the stripe distance of Particle a is 1.2018 Å, corresponding to the (010) plane of NASICON phosphate. The plane distance of Particle b in Fig. 3b2 is 0.4356 Å, which could be attributed to (011) plane of olivine phase. Both vanadium and manganese coexist in the selected particles, whereas Mn and V take leading ratio in olivine and NASICON particles respectively, as presented in Fig. 3a3 & b3, that confirms the synthetic composite as the mixture of $LiMn_{1-y}V_yPO_4$ and $Li_3V_{2-z}Mn_z(PO_4)_3$.

To further affirm the characteristics of microstructure, the synthetic materials were also analyzed with X-ray Photoelectron Spectroscopy (XPS). As shown in Fig. 4, the vanadic spectrum could be divided into two parts, peaked at 517.1 eV representing V in NASICON phase [24] and 515.9 eV probably corresponding to vanadium in olivine. Table 3 lists the mole ratios of two type vanadium, which are very close to the proportion calculated from refinement. This consistency may support the reliability of the refined results. The attempt to distinguish manganese in both phases is unsuccessful for its bonding energy is very close in both phases [25,26].

Fig. 5 shows the charge–discharge curve of the prepared samples at 0.05 C in the potential range of 2.5–4.4 V *vs.* Li/Li^+. As shown in Fig. 5A, plateaus of NASICON phosphates are observable in the composites of $(1-x)$LMP·xLVP/C as $x = 0.03$ and above, which is consistent with XRD results. The discharge plateaus of NASICON phosphate at 3.65 and 3.7 V *vs.* Li/Li^+ are existent in both investigated materials, indicating $Li_3V_2(PO_4)_3$/C could work as DOD's indicator. As the increase of $Li_3V_2(PO_4)_3$ ratio, the discharge capacity is firstly dropped from 99 mAh g^{-1} of 0.99LMP·0.01LVP/C to 69 mAh g^{-1} of 0.95LMP·0.05LVP/C, then augmented to ~120 mAh g^{-1} for the materials of 0.8LMP·0.2LVP/C, and finally stabilized for the composites with more NASICON phase (Fig. 5B). The variation of discharge capacities presents the Plough-shape tendency as the increase of $Li_3V_2(PO_4)_3$ phase, as shown in the inset of Fig. 5B.

Furthermore, the contributions from olivine phase and NASICON phase are calculated based on the refined results. The specific capacity of NASICON phase should be varied very slightly in the investigated composites since the substitution amount is kept between 4–6%. For convenience, the formula of NASICON phosphate

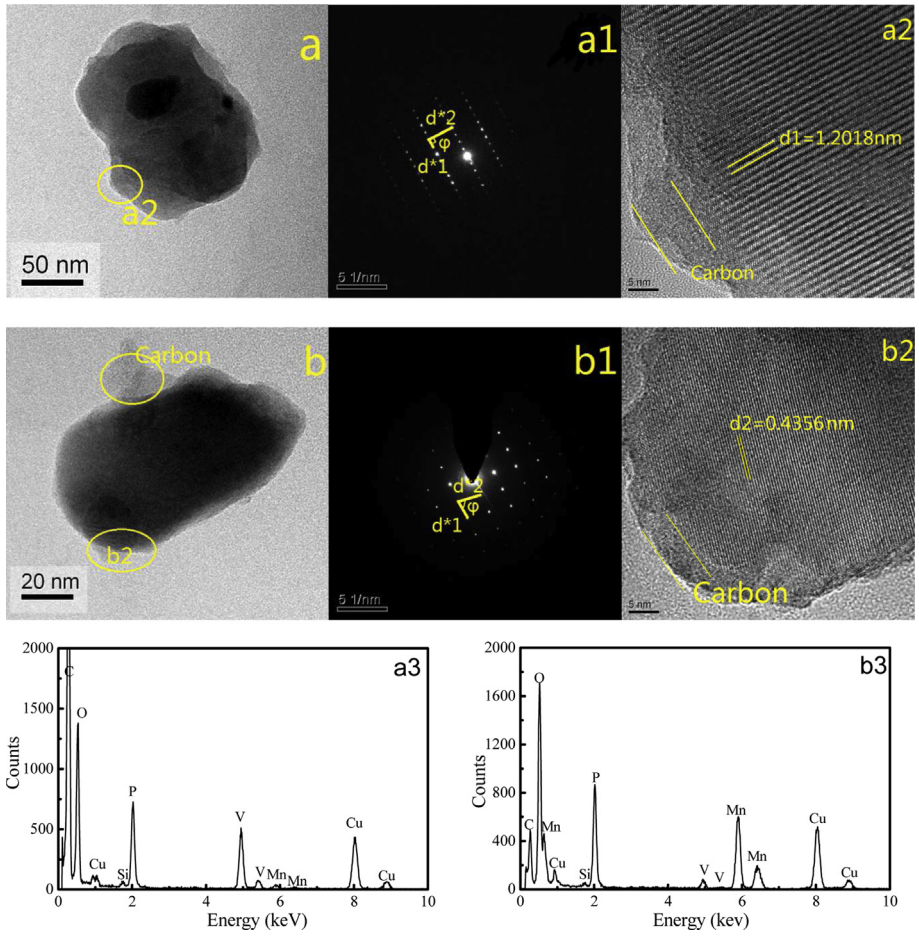

Fig. 3. TEM analysis of 0.6LMP·0.4LVP/C.

is approximated as $Li_3V_{1.95}Mn_{0.05}(PO_4)_3$, which reversible capacity is set as 119 mAh g^{-1} according to Zhai's work [25] and our tested result. As shown in Fig. 5B, only 8% and more vanadium replacement improves the discharge capacity of olivine phase. In the composite level, the improved electrochemical performance was gained by composing 20% $Li_3V_2(PO_4)_3$ by mole, 39.3% by weight, or more, where low-capacity-phase $Li_3V_2(PO_4)_3$ takes a high weight ratio. In addition, the contribution from olivine phase was also weakened since vanadium in $LiMnPO_4$ is electrochemically inactive. Therefore the composites only delivered a moderate discharge capacity.

In this work, the utilization ratio of Mn(II) ↔ Mn(III), instead of discharge capacity, should be more suitable to describe the influence of vanadium substitution on the electrochemical activity of olivine phosphate. This parameter is the quotient of tested discharge capacity over the theoretical capacity, namely $Cap_{test.}/Cap_{theo.}$, with a hypothesis of vanadium electrochemically inactive. The utilization ratio of $Mn^{2+} \leftrightarrow Mn^{3+}$ is 61.6% in the pristine material, decreases to the lowest value 37.6% in 0.9LMP·0.1LVP/C, and augments to more than 90% after composing 30% $Li_3V_2(PO_4)_3$ or more. To understand this abnormal phenomenon, the investigated materials in full discharge state after 12 h equilibrium were characterized with electrochemical impedance spectroscopy (EIS). As shown in Fig. 6, the utilization ratio of Mn(II) ↔ Mn(III) shares the same Plough-shape tendency as the reciprocal of the electrochemical reaction resistance obtained from EIS. It indicates the variance of discharge capacity should be resulted from the resistance of electrochemical reaction, which is influenced by vanadium substitution. The theoretical simulation may be required to further explore the underground reason.

Fig. 7 compares the rate capability of the prepared composite. The composite with 5% $Li_3V_2(PO_4)_3$ exhibits a poor rate behavior,

Table 2
Crystallographic information of the observed particles calculated from SEAD.

Particle	Lattice parameter			Miller index	Crystal plane angle		Phase attribution
		Metrical *d*/nm	Standard *d*/nm		Metrical *φ*/°	Standard *φ*/°	
a	*d*1	1.2018 nm	1.2004 nm	(010)	90.00	90.00	$Li_3V_2(PO_4)_3$
	*d*2	0.3829 nm	0.3833 nm	(201)			
b	*d*1	0.5233 nm	0.5230 nm	(020)	66.23	65.57	$LiMnPO_4$
	*d*2	0.4317 nm	0.4320 nm	(011)			

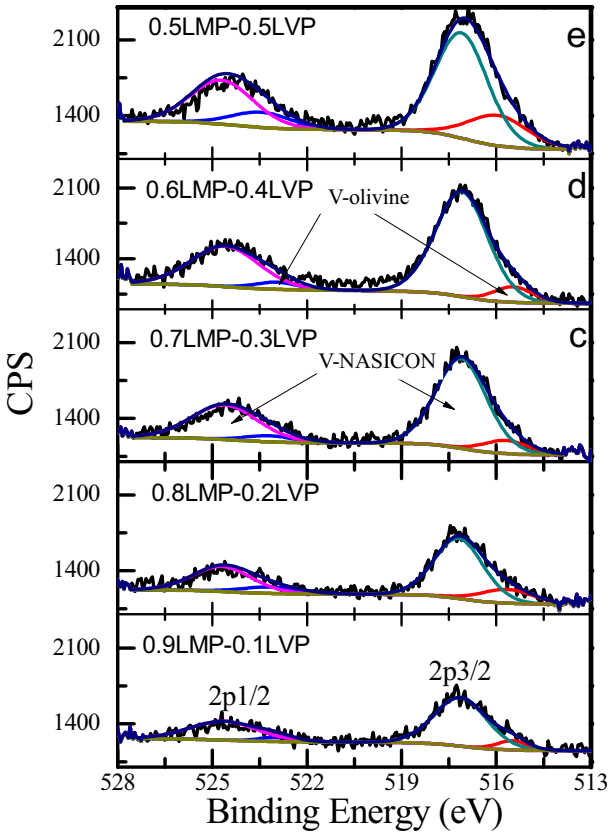

Fig. 4. XPS spectra of vanadium in selected composites.

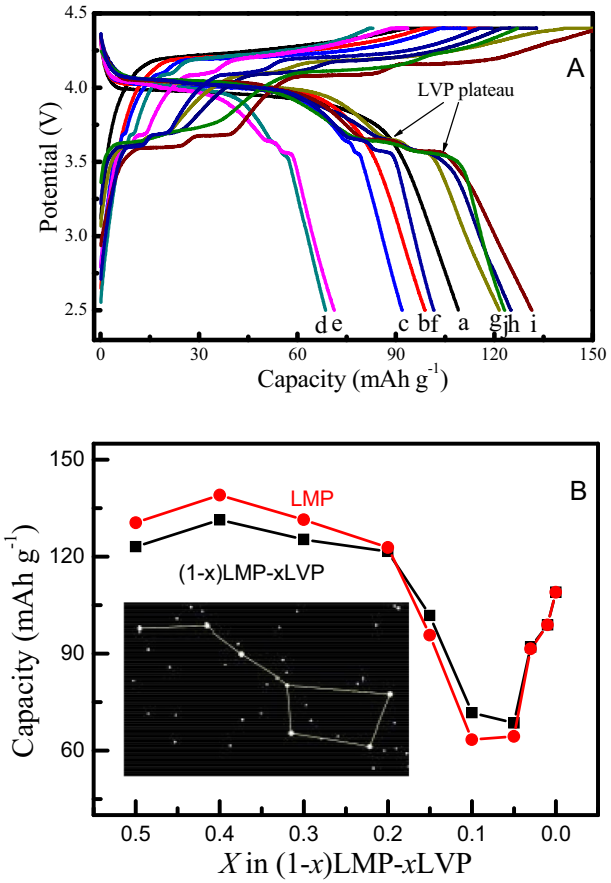

Fig. 5. The initial charge–discharge curves of the samples at 0.05 C. A: the initial charge–discharge curves of (a) $LiMnPO_4$/C, (b) 0.99LMP·0.01LVP/C, (c) 0.97LMP·0.03LVP/C, (d) 0.95LMP·0.05LVP/C, (e) 0.9LMP·0.1LVP/C, (f) 0.85LMP·0.15LVP/C, (g) 0.8LMP·0.2LVP/C, (h) 0.7LMP·0.33LVP/C, (i) 0.6LMP·0.4LVP/C, (j) $Li_3V_2(PO_4)_3$/C; B: influence of the $Li_3V_2(PO_4)_3$ amount on the discharge capacity of $(1-x)$LMP·xLVP and olivine phases. Inset means the star map of the Plough, copied from Google Pictures.

only delivers 69 mAh g^{-1} at 0.05 C and retains 57% at 2 C. The materials with 20–50% $Li_3V_2(PO_4)_3$ present an improved performance in all tested rates. For example, 0.6LMP·0.4LVP/C delivers discharge capacities as high as 131, 129, 125, 122 and 119 mAh g^{-1} at 0.05, 0.1, 0.5, 1 and 2 C, respectively. This variation on rate capability should be dependent on the phase composition, namely substitution amount in olivine phase. The cyclic stability of the prepared samples at 1 C and 2 C is compared in Fig. 8. In contrast to 30% capacity fading of $LiMnPO_4$/C after 500 cycles, the composite of 0.6LMP·0.4LVP/C keeps 89% at 1 C and 86% at 2 C. Obviously, the rate capability and cyclic stability are improved after composing the appropriate amount of $Li_3V_2(PO_4)_3$.

4. Conclusion

The composites of $(1-x)LiMnPO_4 \cdot xLi_3V_2(PO_4)_3$/C have been thoroughly investigated in this work. The plateaus of $Li_3V_2(PO_4)_3$ peaked at 3.65 and 3.70 V *vs.* Li/Li^+ could play the indicative role to warn the end of $MnPO_4 \rightarrow LiMnPO_4$ reaction. In this phosphate composites, olivine component presented an improved performance only after 20% $Li_3V_2(PO_4)_3$ composed, probably corresponding 8% vanadium substitution in olivine phase. The composites as $x = 0.2$–0.5 presented good rate capability and stable cyclic performance with an acceptable capacity of ~125 mAh g^{-1}. It may require another active element, *ca.* Fe, as substituting cation to improve the reversible capacity of olivine $LiMnPO_4$.

Table 3
Ratio of V amount in olivine and NASICON calculated from XPS and XRD.

Nominal ratio of $Li_3V_2(PO_4)_3$	$V_{olivine}/V_{NASICON}$	
	XPS	XRD
10%	0.27	0.28
20%	0.24	0.24
30%	0.26	0.24
40%	0.22	0.24
50%	0.17	0.18

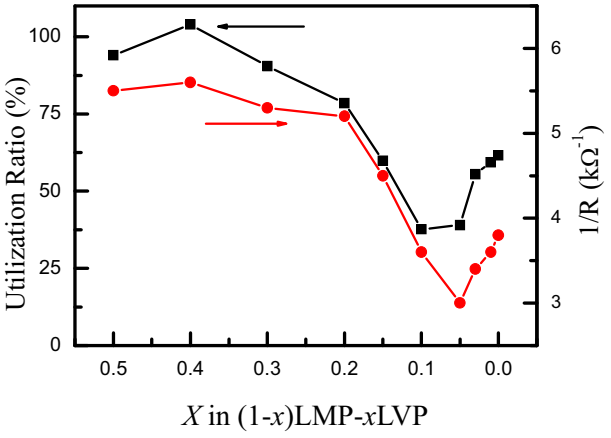

Fig. 6. Tendency of electrochemical reaction resistance and utilization ratio of Mn(II) ↔ Mn(III) as the increase of $Li_3V_2(PO_4)_3$ phase.

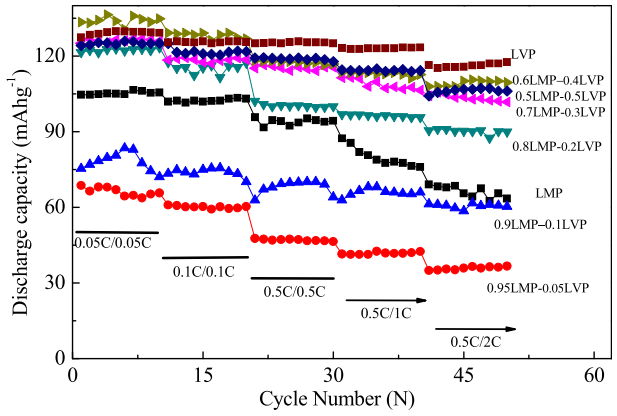

Fig. 7. Rate capability of the prepared composites.

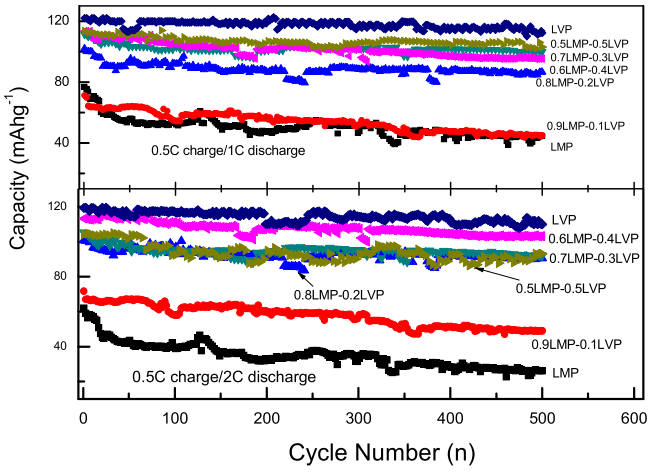

Fig. 8. Cyclic performance of the prepared composites tested under 1 C and 2 C.

Acknowledgments

We are obliged to the financial support of Hundred Talents, Chinese Academy of Science, 973 Program (grant no 2012CB722704), 863 Program (grant no 2013AA050906), Qianjiang Talents (grant no 2012R10078), and Ningbo Key Innovation Team (grant no 2011B82005).

References

[1] M. Armand, J.-M. Tarascon, Nature 451 (2008) 652.
[2] H.Y. Tran, C. Täubert, M. Fleischhammer, P. Axmann, L. Kuppers, M. Wohlfahrt-Mehres, J. Electrochem. Soc. 158 (2011) A556.
[3] A.K. Padhi, K.S. Nanjundaswamy, J.B. Goodenough, J. Electrochem. Soc. 144 (1997) 1188.
[4] G.H. Li, H. Azuma, M. Tohda, Electrochem. Solid-State Lett. 5 (2002) A135.
[5] D. Wang, C. Ouyang, T. Drezen, I. Exnar, A. Kay, N.H. Kwon, P. Gouerec, K.H. Miners, M. Wang, M. Greatzel, J. Electrochem. Soc. 157 (2010) A225.
[6] D. Wang, H. Buqa, M. Crouzet, G. Deghenghi, T. Drezen, I. Exnar, N.-H. Kwon, J.H. Miners, L. Polletto, M. Graetzel, J. Power Sources 189 (2009) 624.
[7] M.Y. Saïdi, J. Barker, H. Huang, J.L. Swoyer, G. Adamson, J. Power Sources 119–121 (2003) 266.
[8] H. Huang, S.-C. Yin, T. Kerr, N. Taylor, L.F. Nazar, Adv. Mater. 14 (2002) 1525.
[9] M.M. Ren, Z. Zhou, X.P. Gao, W.X. Peng, J.P. Wei, J. Phys. Chem. C 112 (2008) 5689.
[10] Y.Q. Qiao, J.P. Tu, Y.J. Mai, J.Y. Xiang, X.L. Wang, C.D. Gu, J. Alloys Compd. 509 (2011) 7181.
[11] Y.Q. Qiao, J.P. Tu, X.L. Wang, C.D. Gu, J. Power Sources 199 (2012) 287–292.
[12] H. Wang, Y.J. Li, C.H. Huang, Y.D. Zhong, S.Q. Liu, J. Power Sources 208 (2012) 282–287.
[13] B. Pei, Z.Q. Jiang, W.X. Zhang, Z.H. Yang, A. Manthiram, J. Power Sources 239 (2013) 475–482.
[14] Y.Q. Qiao, X.L. Wang, Y.J. Mai, J.Y. Xiang, D. Zhang, C.D. Gu, J.P. Tu, J. Power Sources 196 (2011) 8706–8709.
[15] J.T. Xu, S.L. Chou, C.F. Zhou, Q.F. Gu, H.K. Liu, S.X. Dou, J. Power Sources 246 (2014) 124–131.
[16] X.H. Rui, D.H. Sim, K.M. Wong, J.X. Zhu, W.L. Liu, C. Xu, H.T. Tan, N. Xiao, H.H. Hng, T.M. Lim, J. Power Sources 214 (2012) 171–177.
[17] X.D. Guo, B.H. Zhong, H. Liu, Y. Song, J.J. Wen, Y. Tang, Trans. Nonferrous Met. Soc. China 21 (2011) 1761.
[18] J.Y. Xiang, J.P. Tu, L. Zhang, X.L. Wang, Y. Zhou, Y.Q. Qiao, Y. Lu, J. Power Sources 195 (2010) 8331.
[19] P.P. Ma, P. Hu, Z.J. Liu, J.H. Xia, D.G. Xia, Y. Chen, Z.G. Liu, Z.C. Lu, Electrochim. Acta 106 (2013) 187–194.
[20] L. Wang, Z. Li, H. Xu, K. Zhang, J. Phys. Chem. C 112 (2008) 308.
[21] Y. Guo, Y.D. Huang, D.Z. Jia, X.C. Wang, N. Sharma, Z.P. Guo, X.C. Tang, J. Power Sources 246 (2014) 912–917.
[22] G. Yang, H. Ni, H. Liu, P. Gao, H. Ji, S. Roy, J. Pinto, X. Jiang, J. Power Sources 196 (2011) 4747.
[23] F. Wang, J. Yang, Y. NuLi, J. Wang, Electrochim. Acta 103 (2013) 96.
[24] L. Qin, Y. Xia, B. Qiu, H. Cao, Y. Liu, Z. Liu, J. Power Sources 239 (2013) 144.
[25] J. Zhai, M. Zhao, D. Wang, Trans. Nonferrous Met. Soc. China 21 (2011) 523.
[26] D. Choi, J. Xiao, Y.J. Choi, J.S. Hardy, M. Vijayakumar, M.S. Bhuvaneswari, J. Liu, W. Xu, W. Wang, Z. Yang, G.L. Graff, J.-G. Zhang, Energy Environ. Sci. 4 (2011) 4560.